DOI: 10.1002/ejic.200500880

Magnetic Properties of the Ordered Double Perovskite Sr_2MnTeO_6

Luis Ortega-San Martin,[a] Jon P. Chapman,[a] Luis Lezama,[a] Jorge Sánchez Marcos,[c] Jesús Rodríguez-Fernández,[c] María I. Arriortua,[b] and Teófilo Rojo*[a]

Keywords: Perovskite phases / Magnetic structure / EPR spectroscopy / Neutron diffraction

The ordered double perovskite Sr_2MnTeO_6 was prepared by the freeze-drying method. The nuclear and magnetic structures were determined by both X-ray and neutron (D2B and D1B) powder diffraction. A distorted, double perovskite structure type described by the monoclinic $P12_1/n1$ space group is observed at room temperature and down to 4 K. The room temperature EPR spectrum shows an isotropic signal centered at a g value of 1.998 indicating that manganese ions are in the +2 oxidation state. At low temperature the EPR signal broadens as the exchange and dipolar interactions between Mn^{2+} cations increase. Below 25 K no signal is observed, indicating that the sample is magnetically ordered. The dc magnetic susceptibility shows the existence of antiferromagnetic interactions with an ordering temperature around 20 K. A sharp λ-type anomaly observed at 19 K in the specific heat curve and refinement of low-temperature neutron diffraction data confirm the presence of a three-dimensional, antiferromagnetic ordered structure with an ordering temperature of ca. 23 K. The propagation vector of the magnetic structure is $k = [0,0,0]$, yielding a type I antiferromagnetic ordering between Mn^{2+} ($S = {}^5/_2$) cations. At 2 K, each manganese ion is antiferromagnetically aligned to 8 out of 12 nearest-neighbors at an approximate distance of 5.6 Å. This magnetic structure can be viewed as being composed of ferromagnetic arrangement of Mn^{2+} moments in the ab plane, coupled antiferromagnetically along the c axis.

Introduction

Ordered, double perovskites have been of technological interest since the early 1950s when the search for ferroelectric and piezoelectric materials, to be used mainly as capacitors, was extended from the common perovskite oxides, ABO_3 (A being Sr, Ba, Pb, or Ln^{3+} cations and B transition metals), to more complex systems such as the ordered perovskites, $A_2BB'O_6$.[1] As a result, many double perovskites had been discovered and their dielectric properties determined by the mid 1970s.[2] The magnetic and other electrical properties of these ordered perovskites did not attract such interest until the discovery, by Kobayashi et al.[3] in 1998, of room temperature magnetoresistance in the half-metallic Sr_2FeMoO_6 oxide. The intense study in this class of materials carried out after this technologically important discovery has led to the observation of other potentially useful properties such as high temperature superconductivity in $Sr_2YRu_{0.85}Cu_{0.15}O_6$[4] and the coexistence of ferromagnetism and ferroelectricity in Bi_2NiMnO_6.[5]

The magnetic properties, and how the diverse magnetic behaviors depend on the constituent cations, continue to be one of the most important fields of study in these materials. $Sr_2FeB'O_6$ oxides ($B' = Mo^{5+}$ or Re^{5+}) are the best-known examples. These oxides show room temperature ferrimagnetic behavior which results from the incomplete cancellation of the localized Fe moments antiferromagnetically aligned with the delocalized Mo/Re moments, the latter being responsible for the half metallicity and magnetoresistance.[6] If Fe is substituted by Mn, magnetic and electrical behavior changes. $Sr(Mn_{0.5}Ru_{0.5})O_3$ is a partially disordered, ferrimagnetic perovskite with a T_c of approximately 125 K, which also shows magnetoresistive effects. In this phase, however, magnetic exchange is complicated due to the mixed valences observed in the ionic pairs Ru^{IV}/Ru^{V} and Mn^{III}/Mn^{IV}.[7] In other phases, manganese stabilizes as Mn^{2+} leading to higher oxidation states of elements such as Re and Mo than in their Fe analogues, favoring an ordered arrangement of the B and B′ cations. Sr_2MnReO_6, for example, is also ferrimagnetic (arising from an antiferromagnetic coupling between ordered Re and Mn lattices) but has an ordering temperature of 100 K, a low electrical conductivity and shows a poor magnetoresistive effect.[8] Sr_2MnMoO_6 is, by contrast, an antiferromagnetic oxide with a low Néel temperature, of approximately 12 K.[9] In this case, Mn^{2+} is the only paramagnetic cation present, producing a lengthening of the exchange pathways and a

[a] Departamento de Química Inorgánica, Facultad de Ciencia y Tecnología, Universidad del País Vasco (UPV/EHU), Apdo. 644,
48080 Bilbao, Spain
E-mail: teo.rojo@ehu.es
[b] Departamento de Mineralogía y Petrología, Facultad de Ciencia y Tecnología, Universidad del País Vasco (UPV/EHU), Apdo. 644,
48080 Bilbao, Spain
[c] CITIMAC, Facultad de Ciencias, Universidad de Cantabria, 39005 Santander, Spain
Supporting information for this article is available on the WWW under http://www.eurjic.org or from the author.

weakening of the predominantly antiferromagnetic interactions. Below the Néel temperature this phase shows three-dimensional antiferromagnetic order, the observed magnetic structure being of 'type II'.

In the absence of mixed valences and/or vacancy formation, complete cancellation of the antiferromagnetically aligned planes should occur, yielding conventional antiferromagnetic systems with no overall magnetic moment. The magnetic properties reported by Azad et al. for the A_2MnWO_6 (A = Ca, Ba, or Sr) phases,[10] expected to behave in a similar way to the analogous Sr_2MnMoO_6, did not fit, however, with this simple behavior. Low temperature magnetic susceptibility measurements showed the presence of two distinct maxima, the first at ca. 40 K, and the second at temperatures ranging from 9 (A = Ba) to 16 K (A = Ca). The first maximum was attributed to a disordered, canted antiferromagnetic state composed of various domains that, on further lowering of the temperature, undergo a magnetic transition to a three-dimensionally ordered antiferromagnetic phase, also of type II.

Subsequent variable temperature neutron diffraction experiments performed by Muñoz et al.[9a] in samples of the same oxides showed that the Ca and Sr phases are only three-dimensionally ordered below ca. 17 and ca. 14 K respectively, with no intermediate magnetically ordered state between 40 and 20 K. More recently, Lin et al.[11] reported a typical antiferromagnetic behavior for Sr_2MnWO_6 with a unique maximum at ca. 16 K in the magnetic susceptibility curve and no additional features around 40 K. The substitution of Sr cations by La, however, seems to induce in some samples the presence of a small shoulder in the magnetic susceptibility curve and irreversibility in the zero-field cooled/field-cooled susceptibilities also around 40 K.

This diversity of magnetic properties observed in such similar systems highlights the need for detailed studies of the structural and physical properties in related $A_2MnB'O_6$ (B′ = diamagnetic cation) double perovskites, such as those having B′ = Te. We have previously published the room temperature structure and high temperature phase transitions of Sr_2MnTeO_6.[12] In this paper we present the low temperature structure and magnetic properties of this material and establish correlations between structural features and magnetic behavior.

Results and Discussion

Crystal Structure

As previously reported, the room temperature crystal structure of the Sr_2MnTeO_6 ordered double perovskite, refined simultaneously from X-ray and D2B neutron diffraction data, is described by a monoclinic distortion of the ideal cubic cell, in space group $P12_1/n1$.[12] At high temperature, Sr_2MnTeO_6 undergoes three structural phase transitions at approximately 250, 550, and 675 °C, the sequence being $P12_1/n1 \rightarrow I12/m1 \rightarrow I4/m \rightarrow Fm\bar{3}m$, in good agreement with the schemes proposed by Howard and Stokes.[13]

Rietveld refinement of the low temperature crystal structure from high resolution D2B neutron powder diffraction data recorded at 4, 30, and 60 K, showed that the room temperature $P12_1/n1$ symmetry is maintained down to 4 K. The structural model was as previously reported at 298 K (reproduced in Table 1 for comparison), with all atomic positions and isotropic thermal factors freely refined. No mis-site disorder or vacancy formation was observed at 298 K and so was not refined at low temperature. Refined structural parameters are shown in Table 1 and selected bond lengths and angles in Table 2. The Rietveld fits to the 60 and 4 K data are shown in Figure 1. The structure consists of a framework of corner sharing TeO_6 and MnO_6 octahedra, with in phase (+) rotations around the *c* axis and *anti*-phase (–) rotations normal to the *c* axis. The expected increase in the magnitudes of the octahedral rotations and reduction in the cell volume on lowering the temperature are the only significant structural variations.

Table 1. Refined parameters and reliability factors for Sr_2MnTeO_6 from D2B powder diffraction data at different temperatures.

T [K]	298	60	30	4
Symmetry	monoclinic	monoclinic	monoclinic	monoclinic
Space group	$P12_1/n1$	$P12_1/n1$	$P12_1/n1$	$P12_1/n1$
a [Å]	5.7009(1)	5.6887(1)	5.6882(1)	5.6897(1)
b [Å]	5.6770(1)	5.6704(1)	5.6702(1)	5.6719(1)
c [Å]	8.0334(1)	8.0207(1)	8.0201(1)	8.0177(1)
β [°]	90.085(1)	90.091(1)	90.090(1)	90.087(1)
V [Å^3]	259.99(1)	258.73(1)	258.68(1)	258.74(1)
Sr *x*	0.5015(3)	0.5034(4)	0.5034(4)	0.5035(4)
Sr *y*	0.0153(2)	0.0210(3)	0.0212(3)	0.0210(3)
Sr *z*	0.2492(3)	0.2508(4)	0.2507(5)	0.2492(5)
U_{iso} (×100 Å^2)	0.78(2)	0.62(3)	0.60(3)	0.62(3)
Mn *x* = *y* = *z*	0	0	0	0
U_{iso} (×100 Å^2)	0.55(5)	0.7(1)	0.6(1)	0.7(1)
Te *x* = *y*	0	0	0	0
Te *z*	0.5	0.5	0.5	0.5
U_{iso} (×100 Å^2)	0.38(3)	0.51(6)	0.52(6)	0.57(6)
O1 *x*	0.9453(4)	0.9419(4)	0.9418(4)	0.9422(4)
O1 *y*	0.0065(4)	0.0076(3)	0.0080(3)	0.0086(4)
O1 *z*	0.7350(3)	0.7348(3)	0.7349(3)	0.7348(3)
U_{iso} (×100 Å^2)	0.83(5)	0.46(6)	0.47(6)	0.51(7)
O2 *x*	0.2906(4)	0.2935(4)	0.2933(4)	0.2938(4)
O2 *y*	0.2379(5)	0.2348(5)	0.2349(5)	0.2344(5)
O2 *z*	0.9713(4)	0.9701(4)	0.9700(4)	0.9701(4)
U_{iso} (×100 Å^2)	0.91(6)	0.61(6)	0.60(6)	0.74(6)
O3 *x*	0.2591(4)	0.2619(4)	0.2617(4)	0.2620(4)
O3 *y*	0.2126(5)	0.2112(5)	0.2108(5)	0.2096(5)
O3 *z*	0.5283(4)	0.5295(4)	0.5296(4)	0.5296(4)
U_{iso} (×100 Å^2)	1.14(6)	0.87(6)	0.82(6)	0.74(6)
M (Mn)[a]	–	–	–	4.55(2)
R_{wp} [%]	4.7	5.7	5.8	6.4
R_p [%]	3.4	4.2	4.4	4.7
χ^2	2.1	2.0	2.1	2.4
R_F^2	2.9	2.6	2.6	2.0
R_{mag}	–	–	–	4.1

[a] $M_x = 4.55(2)$; $M_y = M_z = 0$.

The high degree of distortion of this phase with respect to the ideal cubic perovskite is a common feature of other similar $Sr_2MnB'O_6$ (B′ = Mo^{6+}, W^{6+}, and Re^{6+}) double perovskites, the structures of which are also described by the $P12_1/n1$ space group (see Table 3). This distortion type

Table 2. Selected bond lengths [Å] and angles [°] of Sr_2MnTeO_6 at various temperatures.

T [K]	298	60	30	4
Mn–O1 x2	2.151(3)	2.153(2)	2.152(2)	2.152(2)
Mn–O2 x2	2.150(2)	2.149(2)	2.149(2)	2.149(2)
Mn–O3 x2	2.145(2)	2.139(2)	2.141(2)	2.146(2)
Mean	2.149	2.147	2.147	2.149
Calcd.[a]	*2.17*			
O1–Mn–O2	90.4(3)	90.3(1)	90.3(1)	90.4(1)
O1–Mn–O3	90.0(2)	90.1(1)	90.2(1)	90.2(1)
O2–Mn–O3	91.6(2)	91.7(1)	91.7(1)	91.6(1)
Te–O1 x2	1.914(3)	1.913(2)	1.914(2)	1.912(2)
Te–O2 x2	1.921(2)	1.923(2)	1.923(2)	1.924(2)
Te–O3 x2	1.921(2)	1.926(2)	1.924(2)	1.921(2)
Mean	1.919	1.921	1.920	1.919
Calcd.[a]	*1.91*			
O1–Te–O2	90.1(1)	90.1(1)	90.1(1)	90.2(1)
O1–Te–O3	90.1(6)	90.0(1)	90.1(1)	90.2(1)
O2–Te–O3	90.30(6)	90.1(1)	90.1(1)	90.2(1)
Mn–O1–Te	162.15(8)	161.1(1)	161.0(1)	161.1(1)
Mn–O2–Te	162.23(7)	160.9(1)	160.9(1)	160.8(2)
Mn–O3–Te	163.29(4)	162.3(2)	162.2(2)	162.0(2)

[a] According to ref.[14]

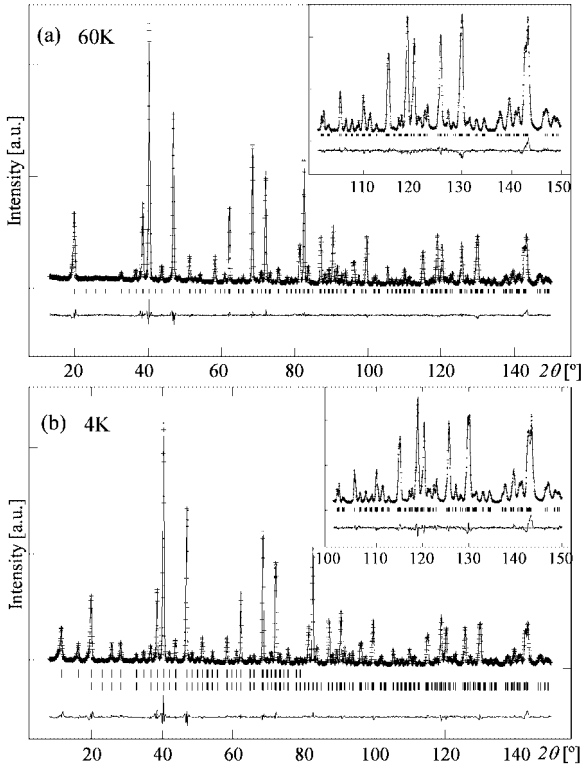

Figure 1. Rietveld fits to the D2B neutron diffraction data at (a) 60 K and (b) 4 K of Sr_2MnTeO_6 in space group $P12_1/n1$, showing observed, calculated and difference curves. Lower and upper reflection markers in (b) correspond to magnetic and nuclear structures, respectively. In each case, the fit to the high angle data is inset.

occurs when the A cation, Sr^{2+} in this case, is too small to fill the space in the three-dimensional network of $B/B'O_6$ octahedra, the result of this mismatch being the tilting of these octahedra around the three axes of the primitive cubic perovskite.

Electron Paramagnetic Resonance Measurements

The room temperature EPR data (see Figure 2, a) show a single, sharp resonance of Lorentzian shape with ΔH_{pp} = 80(1) Oe and a resonance field of 3375.3(2) Oe, corresponding to a g value of 1.998(1). This value of the gyromagnetic factor confirms the oxidation state of Mn as +2 and the sharpness of the resonance is further evidence for the chemical and structural homogeneity of the octahedral Mn environment observed from X-ray and neutron diffraction.

Thermal evolution of the EPR signal was also studied in order to extract information regarding the magnetic and dipolar interactions in the sample. The area of the signal (A_{EPR}) and the peak-to-peak linewidth as a function of temperature are shown in part b of Figure 2. The peak-to-peak linewidth (ΔH_{pp}) can be related to the Mn^{2+} spins' relaxation time, τ, in a way that ΔH_{pp} is proportional to the inverse of τ.[19] As τ usually increases with decreasing temperature we should expect reduction of the signal broadening with lowering temperature. The exchange and dipolar interaction between manganese ions, however, act in the opposite sense. Figure 2 (b) shows that ΔH_{pp} is almost constant down to ca. 30 K indicating that both effects counteract one another. Below 30 K an exponential increase of ΔH_{pp} is observed which indicates that the effect of the exchange interactions between manganese cations is strong and dominates the EPR resonance process. The area of the signal, A_{EPR}, is related to the number of paramagnetic spins and is generally considered as the "EPR susceptibility". In order to avoid errors in the determination of the intensity because of the broadening of the signal into magnetic field regions not covered by the measurements, A_{EPR} was calculated as $Y{\cdot}\Gamma{\cdot}\pi$, which results from double integration of the derivative equation that defines the resonance process for Lorentzian line-shapes.[19] In this expression, Y is the height of the signal and Γ the half-width at half-height, both of which were directly obtained from fits to the experimental data. As shown in part b of Figure 2 the value for A_{EPR} increases monotonically as the temperature is reduced. In order to obtain further information about the type of magnetic interactions, the inverse of the A_{EPR} curve was fitted at high temperatures by a Curie–Weiss law, $\chi = C_m/(T - \theta)$ [see inset (b) in Figure 2] which gave a Weiss constant of ca. –160 K, indicating the presence of antiferromagnetic interactions. Below 25 K, the EPR signal is no longer observed due to significant broadening and reduction in intensity; see the inset (a) in Figure 2. These effects are consistent with the existence of strong magnetic correlations between Mn^{2+} spins below this temperature and the presence of a three dimensionally ordered state (see "Magnetic structure" below).

Magnetic Susceptibility Measurements

Figure 3a shows the temperature dependence of the molar magnetic susceptibility (χ_m) and inverse susceptibility ($1/\chi_m$) curves measured at 1 kOe after cooling without an applied field (ZFC). At high temperature, $T > 150$ K, the

Table 3. Selected structural and magnetic data for several Mn^{2+}-containing ordered perovskites.

	S.G.[a]	T_N	AST[b]	μ_{eff} (μ_B) $T >> T_N$	M (μ_B) $T \approx 4$ K[c]	Ref.
Sr_2MnMoO_6	$P12_1/n1$	12–16	II	$4.5 < \mu_{eff} < 6.28$	4.17(6)	[15,9a]
Sr_2MnWO_6	$P12_1/n1$	≈14	II	5.6	4.54(5)	[9a,10a]
Sr_2MnReO_6	$P12_1/n1$	120[d]	[e]	–	4.49(8)	[16]
Sr_2MnTeO_6	$P12_1/n1$	20	I	6.04	4.54(4)	this work
Ca_2MnWO_6	$P12_1/n1$	16	II	6.19	4.9(1)	[10b]
$LaCaMnNbO_6$	$P12_1/n1$	9	II	6.2	4.69(3)	[17]
Ba_2MnTeO_6	R-3	9	II	6.05	4.75(4)	[18]

[a] Space group. [b] Antiferromagnetic structure type. [c] Refined magnetic moment from neutron diffraction data. [d] In this case, the value refers to T_C. [e] Noncollinear ferromagnetic arrangement.

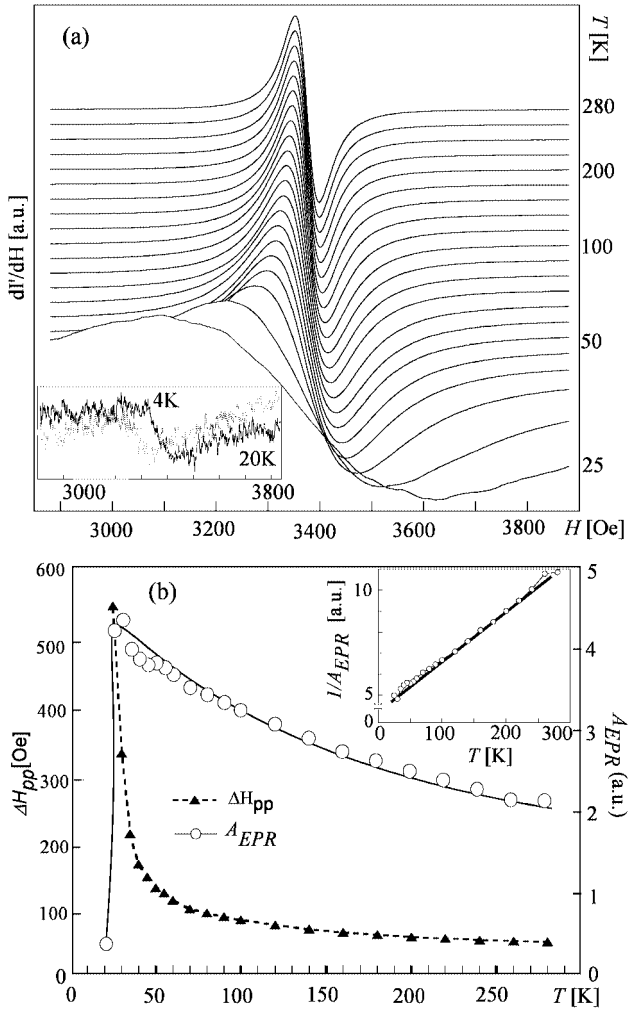

Figure 2. (a) Normalized EPR spectra between 280 and 25 K. The inset shows the weak EPR spectra observed at 4 and 20 K. (b) Thermal evolution of the signal area (A_{EPR}) and the peak-to-peak linewidth (ΔH_{pp}).

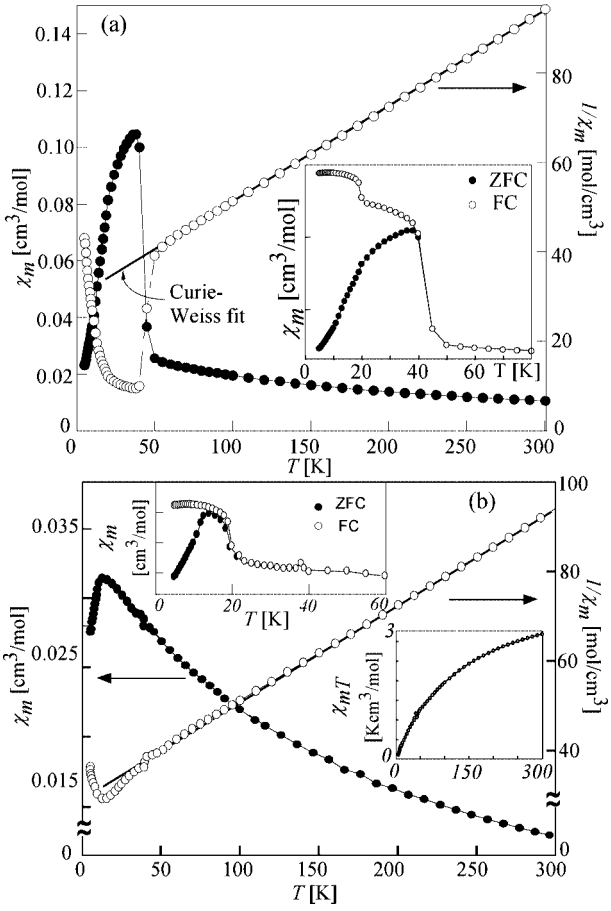

Figure 3. (a) Temperature dependence of the magnetic and reciprocal susceptibilities measured at 1 kOe. The inset shows low temperature details of the ZFC and FC modes of χ_m. (b) Temperature dependence of the magnetic and reciprocal susceptibilities measured at 1 kOe after the subtraction of the component due to the presence of 1.5% by mass of Mn_3O_4. Inset are the corrected ZFC and FC modes and the corrected thermal evolution of the product χ_{mT}.

thermal evolution of χ_m follows the classical Curie–Weiss law, with $C_m = 4.6$ cm^3·K/mol and $\theta = -136$ K indicating that the predominant interactions are of antiferromagnetic nature and in very good agreement with the values obtained from EPR. The effective magnetic moment (μ_{eff}) calculated for the paramagnetic region well above the Néel temperature as $\mu_{eff} = 2.828\sqrt{C_m}$ gave the value of 6.05 μ_B, very close to the theoretical value (5.91 μ_B) obtained from $\mu_{eff} = g\sqrt{S(S+1)}$, considering high spin $S = {}^5/_2$ manganese cations with no orbital contribution.

The inset (a) in Figure 3 shows details of the low-temperature molar magnetic susceptibility (χ_m) measured in ZFC and FC modes. Two distinct features, at approximately 40 and 20 K, can be observed in both modes. The most important characteristic of this low temperature behavior is that the maximum at ca. 40 K appears at the same tempera-

ture as that observed in all A_2MnWO_6 (A = Ca, Ba, Sr) phases studied by Azad et al.,[10] while the low temperature maximum appears at a different temperature in each sample. Similar characteristics have also been observed in phases of the $Sr_{2-x}La_xMnWO_6$ series.[11] It is worth noting that these features observed in some antiferromagnetic manganese-containing double perovskites are very similar to those reported for the ferrimagnetic Mn_3O_4, with a T_c of 42 K.[20]

Field-dependent DC and AC susceptibility measurements, on both Sr_2MnTeO_6 and commercially available Mn_3O_4 (CAS number: 1317-35-7) showed very similar behavior, with the appearance of significant features around 40 K, the only difference being the appearance of a weak maximum in the DC susceptibility and in the real (χ') component of the AC susceptibility in the case of Sr_2MnTeO_6. These characteristics confirm that the maxima around 40 K correspond to Mn_3O_4 rather than originating from the magnetic behavior of Sr_2MnTeO_6. These observed DC susceptibility curves are similar to those reported for the similar double perovskite oxide Ba_2MnWO_6, in which the ferromagnetism observed below 40 K was attributed to a disordered canted antiferromagnetic state composed of various domains.[10c] Further details of the susceptibility study are available as supporting information to this article.

It is worth noting that the presence of undetected Mn_3O_4 has led to misinterpretation of the magnetic properties of many manganese-containing compounds. One of the first examples is the oxide MnO, which was considered to behave as a spin glass around 40 K, but the AC susceptibility revealed that the maximum observed in the DC susceptibility measurements at this temperature actually originated from an undetected fraction of Mn_3O_4.[21] Recently, Goff et al.[22] demonstrated that quantities as low as 1% of this oxide can completely mask the magnetic behavior of the majority phase. The magnetic behavior published for A_2MnWO_6 may be a further example of this type of undetected contamination with Mn_3O_4.[10] The DC susceptibility data for Sr_2MnTeO_6, corrected for an estimated 1.5% by mass of Mn_3O_4 are shown in Figure 3 (b). It is therefore clear that great care must be taken when analyzing the magnetic properties of manganese-containing compounds as manganese oxides exist with strong ferro/ferri-magnetic behavior that, well below the detection limit of other techniques, can completely dominate the magnetic properties of phases under investigation.

Specific Heat Measurements

Figure 4 shows the observed total specific heat (C_P), the calculated contribution of lattice phonons to the specific heat, $C_{P(pho)}$, and the resulting magnetic specific heat, $C_{P(mag)}$. The total specific heat exhibits a three-dimensional (λ-type) magnetic ordering peak at 20 K, in agreement with the previous magnetic and neutron diffraction data. The contribution of the lattice vibrations to the specific heat capacity was calculated by fitting the experimental high temperature data (above the λ anomaly) using a modified Debye model considering the existence of two phonon spectra. For a formula unit containing N atoms, n_1 was assigned a Debye temperature θ_1 and n_2, constrained such that $n_2 = N - n_1$, a Debye temperature θ_2, yielding three independent variables to be refined, namely θ_1, θ_2, and n_1. Refined values indicate that, of the 10 atoms in the formula unit, 3.5 (n_1) have a Debye temperature of 217 K and 6.5 ($n_2 = N - n_1$) have a Debye temperature of 616.5 K. This result not only produces an excellent fit to the experimental data up to 300 K, but is also in good agreement with the chemical formula contents of 4 heavy atoms and 6 light atoms, the latter with a much higher Debye temperature. The magnetic specific heat, $C_{P(mag)}$, shown in Figure 4, being the result of subtracting the phonon component from the total specific heat (C_P).

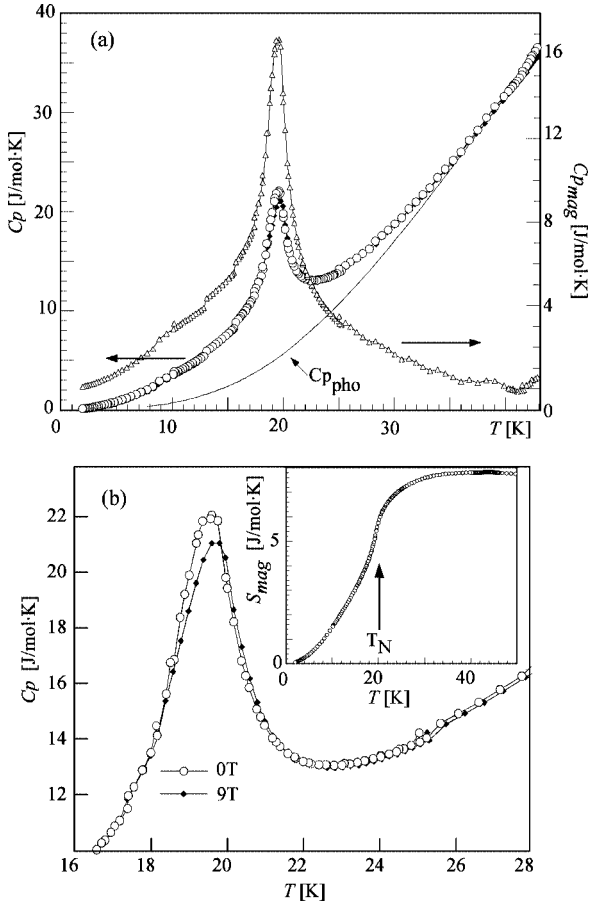

Figure 4. (a) Specific heat vs. temperature of Sr_2MnTeO_6 from 1.8 to 45 K showing total specific heat, Cp, the calculated phonon contribution, Cp_{pho}, and the resultant magnetic contribution, Cp_{mag}. (b) Comparison between the specific heat data measured at 0T and under an applied magnetic field of 9T. The inset shows the calculated magnetic entropy, S_{mag}.

The effect of a 9T magnetic field on the three-dimensional λ peak in the heat capacity is shown in Figure 4 (b). In a pure antiferromagnetic sample, a small displacement of the peak to lower temperatures with increasing magnetic

field would be expected. It can be seen, however, that the peak is slightly displaced to higher temperature with the applied field, indicating a small ferromagnetic component. This ferromagnetic component may originate from a small canting in the antiferromagnetic structure as the small magnitude of the displacement is typical of highly anisotropic antiferromagnets. The thermal evolution of the magnetic entropy, S_{mag}, released in the ordering process for this phase is shown in the inset (b) of Figure 4. The total magnetic entropy, calculated from the $S_{mag}(T) = \int_0^T C_{mag}(T)/T \cdot dT$ expression, was found to be ≈8 J/mol·K above 20 K. This value is ≈60% of the theoretical value, $R \cdot \ln(2S + 1)$ = 14.9 J/mol·K, expected for the $S = {}^5/_2$ state of the Mn^{2+} cation at low temperatures. This low value could be related to systematic errors in the subtraction of the lattice component around the observed maximum in the specific heat data or, as has been previously suggested, this deviation could indicate that some of the spins of the Mn^{2+} ions are not correlated to the rest.[23] The latter explanation would, however, also imply a similar deviation of the low temperature magnetic moment of the Mn^{2+} spins, an effect not observed in Sr_2MnTeO_6.

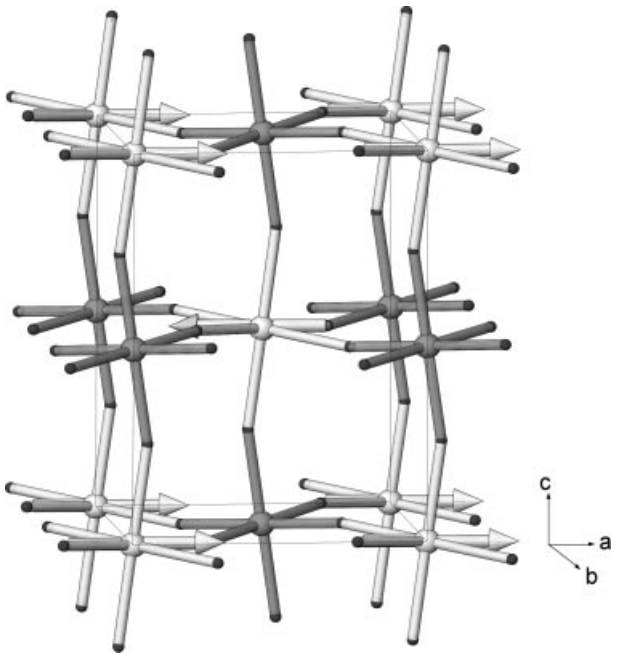

Figure 5. Type I antiferromagnetic structure of Sr_2MnTeO_6. Lighter spheres represent Mn and darker spheres Te. Sr atoms are omitted for clarity.

Magnetic Structure

The 4 K neutron diffraction data show the presence of several additional peaks which arise from long-range magnetic order in the sample (see Figure 1, b). These reflections were not coincident with those of the nuclear structure indicating that this magnetic order is of antiferromagnetic nature. These peaks were indexed considering a magnetic cell with the same dimensions as that of the crystal cell (with parameters $\sqrt{2}a_p \times \sqrt{2}a_p \times 2a_p$, where a_p is the primitive cubic perovskite parameter) in the $P1$ space group (refined neutron data are shown in Figure 1, b). The first two sharp magnetic peaks are, consequently, the unique (001) reflection and the unresolved doublet composed of the (010) and (100) reflections. The type I antiferromagnetic structure is the only collinear arrangement of magnetic ions compatible with these observed maxima. The strong (001) peak indicates that an important component of the magnetic moment is in the *ab* plane. The orientation of the magnetic moments in this plane could not be determined, because of the overlap of the (010) and (100) reflections. No significant component was observed in the *c*-direction. In the final model, magnetic moments of magnitude *M*, were fixed along *a* and –*a* in alternating planes in the *c*-direction. The refined structure at 4 K, showing the orientation of magnetic moments, is shown in Figure 5. In this magnetic structure each manganese cation is antiferromagnetically coupled by 90° superexchange interactions via diamagnetic –O–Te^{6+}–O– bridges to 8 out of 12 nearest-neighbors, NN, at an approximate distance of 5.6 Å. The six next nearest-neighbors, NNN, (at ca. 8.0 Å) are all ferromagnetically aligned via 180° –O–Te^{6+}–O– linkages.

Figure 6 shows the temperature-dependent D1B diffraction data. The thermal evolution of the refined magnetic moment (M_x) is represented in Figure 7. It can be observed that the three-dimensional magnetic order begins at 20 K. The Mn^{2+} moment rapidly increases below 20 K, reaching saturation at approximately 10 K. The obtained value of M_x = 4.55(5) μ_B is close to the theoretical value of 5 μ_B for high spin $S = {}^5/_2$ manganese at low temperature.

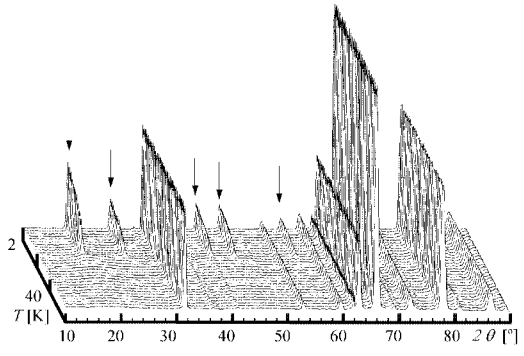

Figure 6. Temperature-dependent D1B neutron diffraction data from 2 to 60 K. Magnetic peaks are marked by arrows.

The temperature dependence of the refined lattice parameters and volume are shown in Figure 8. The thermal evolution of the lattice parameters is of particular interest. The *a* parameter exhibits almost no variation whereas the *b* and *c* parameters show different behaviors with temperature. Below 20 K, where three-dimensional magnetic order is observed, the parameters show no systematic change. At 20 K, a marked discontinuity is observed in both parameters with *c* increasing and *b* decreasing. Above 20 K, the *b* and *c* parameters are again virtually independent of tem-

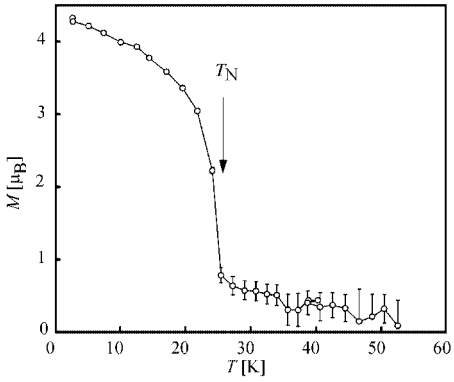

Figure 7. Temperature dependence of the magnitude of the magnetic moment refined from D1B neutron diffraction data from 2 to 60 K, with the Néel temperature, T_N = 22 K, marked.

perature. The thermal evolution of the unit cell volume shows no change below 20 K and a small increase at higher temperatures.

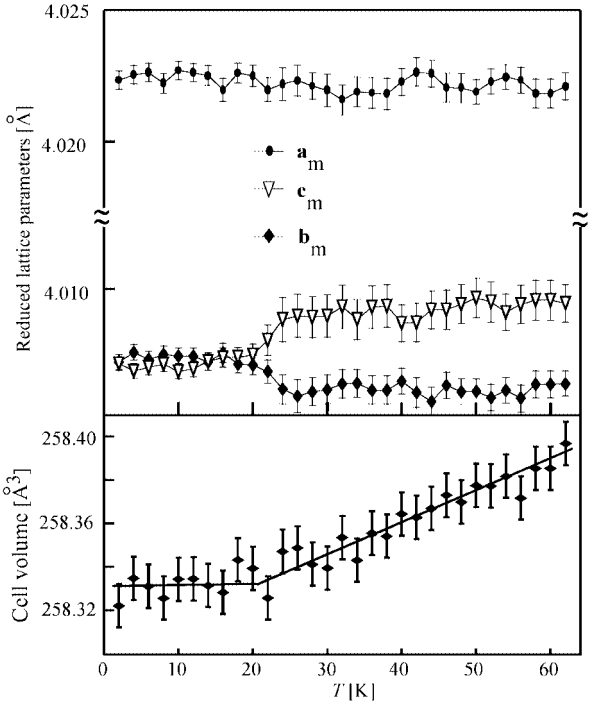

Figure 8. Temperature dependence of the reduced lattice parameters and cell volume refined from D1B neutron diffraction data from 2 to 60 K. Reduced lattice parameters were calculated as follows: $a_m = a/\sqrt{2}$, $b_m = b/\sqrt{2}$; cm = c/2.

The observed behavior could be associated to "spontaneous magnetostriction" resulting from a magnetically ordered state, in contrast to the "common magnetostriction" effect that results from the application of a magnetic field.[24] In Sr_2MnTeO_6, this effect can be viewed as the result of the nature of the magnetic order (see Figure 9), where moments perpendicular to the [001] direction attract one another, leading to a reduction of the c parameter with the increase in b parameter being the result of the repulsion between ferromagnetically aligned moments in the ab plane. Similar, but more pronounced, spontaneous magnetostriction effects have also been recently observed in the ferromagnetic oxides $SrRu_{1-x}O_3$.[25a] Field-induced magnetostriction is common in other ferromagnetic perovskites, such as manganites and double perovskites,[25b–25c] but the observation of this spontaneous effect in this type of antiferromagnet is rare.

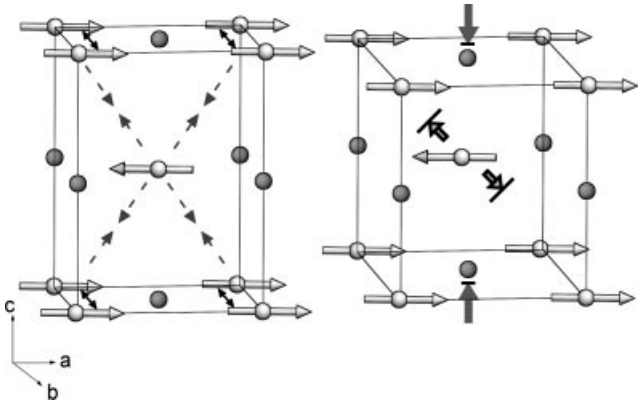

Figure 9. Origin of the spontaneous magnetostriction effect observed in Sr_2MnTeO_6. Dark spheres represent Te and light ones with arrows represent Mn with their magnetic moments. Also depicted are arrows indicating the compressions and elongations of the unit cell dimensions as a consequence of the magnetic ordering. Sr and O atoms are omitted for clarity.

Conclusions

The ordered double perovskite Sr_2MnTeO_6 crystallizes at room temperature in space group $P12_1/n1$ and maintains its symmetry on cooling down to 4 K. Electron paramagnetic resonance spectroscopy shows the presence of a sharp resonance centred at a g value of 1.998(2), indicating that manganese ions are in the +2 oxidation state. As the temperature is lowered and magnetic exchange interactions between Mn^{2+} become stronger, the area of the resonance increases showing a maximum around 25 K. Below this temperature a large broadening of the signal occurs indicating that the sample is magnetically ordered.

Magnetic DC susceptibility follows the Curie–Weiss law at high temperatures, and a Weiss constant of –136 K indicates that the predominant interactions are of antiferromagnetic nature. The observed effective magnetic moment agrees well with a $S = {}^5/_2$ cation with no orbital contribution. The Néel temperature was estimated to be 20 K. At this same temperature the specific heat shows a λ-type anomaly typical of three-dimensionally ordered systems, which is slightly repressed on application of a field of 9T. Both effects are consistent with the observed anti-ferromagnetic ordering within the sample. Low temperature neutron diffraction indicates that the ordered antiferromagnetic state is of type I, in which planes perpendicular to the (001) direction contain $S = {}^5/_2$ Mn^{2+} magnetic moments ferromagnetically coupled to one another within the plane via diamagnetic –O–Te^{6+}–O– bridges. These planes are coupled antiferromagnetically because of the stronger 90° Mn–

O···O–Mn linkages, producing the predominant antiferromagnetic inter-planar interactions. The observed magnetic moment per manganese ion of 4.5 μ_B indicates that virtually all the sample is magnetically ordered at this temperature. Discontinuities observed around the ordering temperature in the lattice parameters indicate that this phase also shows a small spontaneous magnetostriction effect.

Experimental Section

Synthesis, room temperature structural refinement, and confirmation of nominal stoichiometry of the ordered double perovskite Sr_2MnTeO_6 have been reported previously.[12] Low temperature neutron powder diffraction data were collected at 4, 30, and 60 K on instrument D2B at the Institut Laue Langevin (I.L.L.), Grenoble, France. Neutrons of wavelength 1.595 Å were incident on 10 g of Sr_2MnTeO_6, contained in an 8-mm diameter vanadium can held in a liquid helium cryostat. Data were collected over the angular range $0 \leq 2\theta \leq 160°$, then normalized for subsequent refinement in GSAS.[26]

Temperature-dependent neutron powder diffraction data were collected on instrument D1B at the I.L.L. Neutrons of wavelength 2.52 Å were incident on 10 g of Sr_2MnTeO_6, contained in an 8-mm diameter vanadium can held in a liquid helium cryostat. Data were collected every 2 K from 2 to 60 K over the angular range $10 \leq 2\theta \leq 90°$. Evolution of lattice parameters and magnetic moment (M_x) with temperature were obtained by sequential refinement in FullProf[27] starting from the structural model refined with D2B data at 4 K.

X-band EPR spectra were recorded between 0 and 7 kOe from 300 to 5 K with a Bruker ESP 300 spectrometer. The temperature was controlled by an Oxford Instruments (ITC4) regulator. The magnetic field was measured with a Bruker BNM 200 gaussmeter and the frequency inside the cavity was determined using a Hewlett–Packard 5352B microwave frequency counter.

DC magnetic susceptibility measurements were performed using a Quantum Design MPMS-7 SQUID magnetometer whilst heating from 5 to 300 K in an applied field of 1 and 5 kOe. In both cases, data were collected after cooling either in the presence (field cooling –FC curve) or absence (zero-field cooling- ZFC curve) of the applied field. Magnetization as a function of applied field (H) was measured using the same MPMS-7 SQUID magnetometer after cooling the sample in zero field. Magnetization was also measured as a function of temperature between 5 and 80 K.

AC magnetic susceptibility measurements were made with a standard QD PPMS system with an alternate excitation field (H_{ac}) of 1 Oe at frequencies between 10^2 and 10^4 Hz. Data were recorded from 4 to 60 K as a function of both frequency and applied DC magnetic field.

Heat capacity measurements were carried out by a relaxation method using the same PPMS system. The sample was a plate of 0.3 mm thickness and 7 mg weight obtained by compressing the original powder. Data were collected with zero field (0T) and under an applied field of 9T from 1.8 to 300 K.

Supporting Information (for details see the footnote on the first page of this article): Further magnetic data are available as Supporting Information, due to the magnetic characterisation of Sr_2MnTeO_6 having been complicated by the presence of the ferromagnetic oxide, Mn_3O_4. Field-cooled and zero-field cooled DC susceptibilities at various applied fields and field- and frequency-dependent AC susceptibilities are presented for both the as-prepared Sr_2MnTeO_6 and commercially available Mn_3O_4. Also included is the field-dependence of the magnetization for Sr_2MnTeO_6.

Acknowledgments

This work has been funded by the "Ministerio de Ciencia y Tecnología (MCyT)" (projects MAT2004-02425 and MAT2002-04178-C04-04). L.O.-S.M acknowledges MCyT for a Doctoral Fellowship and J.P.C. thanks MCyT for funding (MAT, 2001-0064). Prof. J.P. Attfield of the University of Edinburgh is acknowledged for fruitful magnetic discussions. The authors gratefully acknowledge Dr. G. Cuello for assistance with data collection at the I.L.L., Grenoble, France and the I.L.L. for provision of beam-time on instruments D2B and D1B.

[1] F. Galasso, *Perovskites and High Tc superconductors*, Gordon & Breach, New York, **1990**.
[2] M. T. Anderson, K. B. Greenwood, G. A. Taylor, K. R. Poeppelmeier, *Prog. Solid State Chem.* **1993**, *22*, 197–233.
[3] K.-I. Kobayashi, T. Kimura, H. Sawada, K. Terakura, Y. Tokura, *Nature* **1998**, *395*, 677–680.
[4] H. A. Blackstead, J. D. Dow, D. R. Harshman, W. B. Yelon, M. X. Chen, M. K. Wu, D. Y. Chen, F. Z. Chien, D. B. Pulling, *Phys. Rev. B* **2001**, *61*, 214412.
[5] M. Azuma, K. Takata, T. Saito, S. Ishiwata, Y. Shimakawa, M. Takano, *J. Am. Chem. Soc.* **2005**, *127*, 8889–8892.
[6] a) D. D. Sarma, *Curr. Opin. Solid State Mater. Science* **2001**, *5*, 261–268; b) O. Chmaissem, R. Kruk, B. Dabrowski, D. E. Brown, X. Xiong, S. Kolesnik, J. D. Jorgensen, W. C. Kimball, *Phys. Rev. B* **2000**, *62*, 14197–14206; c) H. Kato, T. Okuda, Y. Okimoto, T. Tomioka, K. Oikawa, T. Kamiyama, Y. Tokura, *Phys. Rev. B* **2004**, *69*, 184412.
[7] R. K. Sahu, S. Sundar-Manoharan, *J. Appl. Phys.* **2002**, *92*, 4831–4833.
[8] G. Popov, M. V. Lobanov, E. Tsiper, M. Greenblatt, E. Caspi, A. Borisov, V. Kiryukhin, J. Lin, *J. Appl. Phys.* **2004**, *16*, 135–145.
[9] a) A. Muñoz, J. A. Alonso, M. T. Casais, M. J. Martínez-Lope, M. T. Fernández-Díaz, *J. Phys.: Condens. Matter* **2002**, *14*, 8817–8830; b) M. Itoh, I. Ohta, Y. Inaguma, *Mater. Science Eng. B* **1996**, *41*, 55–58.
[10] a) A. K. Azad, S. A. Ivanov, S.-G. Eriksson, H. Rundölf, J. Eriksen, R. Mathieu, P. Svedlindh, *J. Mag. Mag. Mater.* **2001**, *237*, 124–134; b) A. K. Azad, S. A. Ivanov, S.-G. Eriksson, J. Eriksen, H. Rundölf, R. Mathieu, P. Svedlindh, *Mater. Res. Bull.* **2001**, *36*, 2485–2496; c) A. K. Azad, S. A. Ivanov, S.-G. Eriksson, J. Eriksen, H. Rundölf, R. Mathieu, P. Svedlindh, *Mater. Res. Bull.* **2001**, *36*, 2215–2228.
[11] Q. Lin, M. Greenblatt, M. Croft, *J. Solid State Chem.* **2005**, *178*, 1356–1366.
[12] L. Ortega-San Martín, J. P. Chapman, E. Hernández-Bocanegra, M. Insausti, M. I. Arriortua, T. Rojo, *J. Phys.: Condens. Matter* **2004**, *16*, 3879–3888.
[13] C. J. Howard, H. T. Stokes, *Acta Crystallogr. Sect. A* **2005**, *61*, 93–111.
[14] R. D. Shannon, *Acta Crystallog. A* **1976**, *32*, 751–767.
[15] A. K. Azad, S.-G. Erikson, S. A. Ivanov, R. Mathieu, P. Svendlindh, J. Eriksen, H. J. Rundölf, *J. Alloys Comp.* **2004**, *364*, 77–82.
[16] a) H. Kato, T. Okuda, Y. Okimoto, Y. Tomioka, K. Oikawa, T. Kamiyama, Y. Tokura, *Phys. Rev. B* **2004**, *69*, 184412; b) G. Popov, M. V. Lobanov, E. Tsiper, M. Greenblatt, E. Caspi, A. Borissov, V. Kiryukhin, J. Lynn, *J. Phys.: Condens. Matter* **2004**, *16*, 135–145.
[17] J.-W. G. Bos, J. P. Attfield, *Z. Anorg. Allg. Chem.* **2004**, *630*, 2248–2252.

[18] L. Ortega-San Martín, J. P. Chapman, L. Lezama, M. I. Arriortua, T. Rojo, *Abstracts of the Solid State Chemistry Conference (SSC2004)*, Academy of Science of the Czech Republic, Prague, September **2004**.
[19] a) F. E. Mabbs, D. Collison, *Electron Paramagnetic Resonance of d Transition Metal Compounds*, Elsevier, Amsterdam, **1992**; b) J. A. Weil, J. R Bolton, J. E. Wertz, *Electron Paramagnetic Resonance – Elementary Theory and Practical Applications*, John Wiley & Sons, New York, **1994**.
[20] W. S. Seo, H. H. Jo, K. Lee, B. Kim, S. J. Oh, J. T. Park, *Angew. Chem. Int. Ed.* **2004**, *43*, 1115–1117.
[21] J. J. Hauser, J. V. Waszczak, *Phys. Rev. B* **1984**, *30*, 5167–5171.
[22] R. J. Goff, A. J. Williams, J. P. Attfield, *Phys. Rev. B* **2004**, 014426.
[23] K. Boulahya, M. Parras, J. M. González Calbet, U. Amador, J. L. Martínez, M. T. Fernández-Díaz, *Phys. Rev. B* **2004**, *69*, 024418.
[24] A. del Moral, P. A. Algarabel, J. I. Arnaudas, L. Benito, M. Ciria, C. de la Fuente, B. García-Landa, M. R. Ibarra, C. Marquina, L. Morellón, J. M. de Teresa, *J. Magn. Magn. Mater.* **2002**, *242–245*, 788–796.
[25] a) B. Dabrowski, M. Avdeev, O. Chmaissem, S. Kolesnik, P. W. Klamut, M. Maxwell, J. D. Jorgensen, *Phys. Rev. B* **2005**, *71*, 104411; b) R. Mahendiran, M. R. Ibarra, C. Marquina, B. Garcia-Landa, L. Morellon, A. Maignan, B. Raveau, A. Arulraj, C. N. R. Rao, *Appl. Phys. Lett.* **2003**, *82*, 242–244; c) D. Serrate, J. M. De Teresa, P. A. Algarabel, C. Marquina, L. Morellon, J. Blasco, M. R. Ibarra, *J. Magn. Magn. Mater.* **2005**, *290–291*, 843–845.
[26] A. C. Larson, R. B. Von Dreele, "*GSAS*: General Structure Analysis System", Los Alamos National Laboratory Report LAUR 86–748, **1994**.
[27] J. Rodriguez-Carvajal, "*FULLPROF*: A Program for Rietveld Refinement and Pattern Matching Analysis", Abstracts of the Satellite Meeting on Powder Diffraction of the XV Congress of the IUCr, p. 127, Toulouse, France, **1990**.

Received: September 30, 2005
Published Online: February 6, 2006

